Environmental Pollution 242 (2018) 667–674

Contents lists available at ScienceDirect

Environmental Pollution

journal homepage: www.elsevier.com/locate/envpol

Emission factors of particulate and gaseous compounds from a large cargo vessel operated under real-world conditions☆

Cheng Huang [a, *], Qingyao Hu [a], Hanyu Wang [b], Liping Qiao [a], Sheng'ao Jing [a], Hongli Wang [a], Min Zhou [a], Shuhui Zhu [a], Yingge Ma [a], Shengrong Lou [a], Li Li [a, **], Shikang Tao [a], Yingjie Li [a], Diming Lou [c]

[a] State Environmental Protection Key Laboratory of Cause and Prevention of Urban Air Pollution Complex, Shanghai Academy of Environmental Sciences, Shanghai, 200233, China
[b] School of Naval Architecture, Ocean & Civil Engineering, Jiaotong University, Shanghai, 200240, China
[c] School of Automobile Studies, Tongji University, Shanghai, 201804, China

ARTICLE INFO

Article history:
Received 23 March 2018
Received in revised form
14 June 2018
Accepted 9 July 2018
Available online 17 July 2018

Keywords:
Ship emissions
Emission factors
PM components
VOC species
On-board measurement

ABSTRACT

On-board emissions measurements were performed on a Handysize-class bulk carrier operating under real-world conditions. Emission factors (EFs) were determined for criteria pollutants such as NO_x, CO, total hydrocarbons (THC), and PM; PM composition, including organic and elemental carbon (OC and EC), inorganic species, and a variety of organic compounds and VOC species (including alkanes, alkenes, single-ring aromatics, and oxygenated VOCs) were also analyzed. To investigate the impacts of engine type, fuel, and operating conditions on emissions, measurements were conducted on one main and one auxiliary engines using low- and high-sulfur fuels (LSF and HSF) under actual operating conditions, including at-berth, maneuvering, and cruising at different engine loads. OC was the most abundant PM component (contributing 45–65%), followed by sulfate (2–15%) and EC (1–20%). Compounds with 3 or 4 aromatic rings, including phenanthrene, fluoranthene, pyrene, and benzo[b+k]fluoranthene, dominated the particulate polycyclic aromatic hydrocarbons (PAHs) emitted from the ship, accounting for 69–89% of the total PAHs. Single-ring aromatics constituted 50–78% of the emitted VOCs and were dominated by toluene. In this study, switching from HSF (1.12% S) to LSF (0.38% S) reduced emitted PM by 12%, OC by 20%, sulfate by 71%, and particulate PAHs by 94%, but caused an increase in single-ring aromatics. The power-based EFs generally decreased with increasing engine loads. However, decreasing the ship engine load also reduced the vessel speed and, thus, decreased emissions over a given voyage distance. Herein, a Vessel Speed Reduction (VSR) from 11 to 8–9 knots decreased NO_x and PM emissions by approximately 33% and 36%, respectively, and OC, EC, sulfate, and particulate PAHs in PM emissions by 34%, 83%, 29%, and 11%. These data can be used to minimize uncertainty in the emission factors used in ship emissions calculations.

1. Introduction

Particulate and gaseous emissions from ships have attracted increasing attention for their potential impacts on air quality (Gaston et al., 2013; Aksoyoglu et al., 2016; Marelle et al., 2016; Becagli et al., 2017; Liu et al., 2017), climate change (Olivié et al., 2012; Liu et al., 2016), and human health (Brandt et al., 2013; Broome et al., 2016). Particulate matter (PM) emitted from ships consists of a number of components, including carbonaceous substances, inorganic salts (such as sulfate and nitrate salts), organic compounds, and metals, that can greatly impact visibility (Seinfeld and Pandis, 2006; Pitchford et al., 2007). PM also participates strongly in climate forcing through both direct and indirect effects (Lack et al., 2011; Thomson et al., 2018). The organic fraction emitted from ships may contain a number of toxic components, including polycyclic aromatic hydrocarbons (PAHs), which possess mutagenic and carcinogenic properties and pose a significant risk to human health (Diesch et al., 2013; Czech et al., 2017; Manoli

☆ This paper has been recommended for acceptance by Charles Wong.
* Corresponding author.
** Corresponding author.
E-mail addresses: huangc@saes.sh.cn (C. Huang), lili@saes.sh.cn (L. Li).

https://doi.org/10.1016/j.envpol.2018.07.036
0269-7491/

et al., 2017). Due to increasing emissions of NO_x and volatile organic compounds (VOCs) from ships, ship emissions may explain, at least in part, the high ozone concentrations measured in air masses with marine back-trajectory origins (Eyring et al., 2010; Velchev et al., 2011; Tagaris et al., 2017). However, measurements of VOCs from ships are relatively few, which may hinder VOC ozone formation potential calculations.

Ocean-going cargo vessels, including container ships, cargo carriers, tankers, etc., contribute significantly to global air pollutant emissions from ships, accounting for 84, 88, and 87% of global marine NO_x, SO_x, and $PM_{2.5}$ emissions, respectively (Johansson et al., 2017). Ocean-going cargo vessels are primarily fueled with heavy fuel oil (HFO). Currently, vessels are required to switch from HFO to distillate fuel (DF) in sulfur emission control areas (SECAs) to satisfy sulfur regulations. However, the SECAs are generally limited to Europe and some parts of North America, and vessels in other areas use predominantly HFO. Global HFO consumption totaled ~195 million tons in 2015, constituting 71% of the total fuel consumption for global shipping, and has been increasing at a rate of 2.1% per year (Johansson et al., 2017). Previous research has indicated that emissions of unregulated hazardous species with air quality and human health impacts (e.g., sulfate, OC species, PAHs, and transition metals) are significantly higher from HFO than from DF at all engine loads (Sippula et al., 2014).

Measurements of ship EFs for particulate and gaseous components are essential for compiling emission inventories and quantifying the impacts of emissions on air quality, climate change, and human health. In the last decade, numerous measurement campaigns have been conducted to determine EFs for ocean-going vessels. The EFs measured for regulated pollutants such as SO_2 and NO_x (Agrawal et al., 2008a, 2008b; 2010; Khan et al., 2013) are comparable to Lloyds service data (ENTEC, 2002) and EF estimates from the USEPA (2009) and CARB (2008). Recent studies have also focused on emissions of unregulated chemical compounds (Agrawal et al., 2008a, 2008b; Moldanová et al., 2013); correlations between such compounds and various fuel types (Jayaram et al., 2011; Lack et al., 2011; Celo et al., 2015), engine loads (Agrawal et al., 2010; Sippula et al., 2014), and after-treatment technologies (Lack and Corbett, 2012; Lehtoranta et al., 2015) have been discussed in previous studies. However, in comparison to on-road vehicles, emissions of particulate and gaseous species from HFO-fueled vessels remain poorly understood, especially under real-world operating conditions.

In this study, the EFs of particulate and gaseous species were determined for a large, modern bulk carrier via on-board measurements at sea. Measurements were performed during all of the operational modes typically experienced over the course of a voyage, including at-berth, departure, ocean and inland cruising, and arrival. Several different cruise speeds were designated to investigate the impact of cruise speed on the EFs of particulate and gaseous species.

2. Materials and methods

2.1. Emission measurement campaign

The measurements were performed in July 2017 on a large cargo vessel during an actual sea voyage. The ship, a Handysize-class bulk carrier, was built in 2012 and features a deadweight of 45,308 t and gross tonnage of 31,113 t. The ship is equipped with one main engine, four auxiliary engines, and an auxiliary boiler. In this study, emissions were measured from one main engine and one auxiliary engine; the major technical specifications of the main and auxiliary engines are presented in Table 1. The ship used RMG 180 grade HFO for both the main and auxiliary diesel engines. China has executed legislation that requires ships to use LSF (<0.5 wt% S) when at berth beginning January 1, 2017. Therefore, the engines burned LSF with 0.38 wt% S when at berth and during departure; HSF with 1.12 wt% S was burned during other operational modes. It should be noted that the fuel sulfur content limit in Chinese SECAs (<0.5%) is quite a bit looser than the limits in North America and Europe (0.1%). Therefore, the LSF used in this study differs from the DF used in emission control areas in North America and Europe; the physico-chemical properties (e.g., metal and asphaltene content, viscosity, etc.) of the LSF used herein are not fundamentally superior to those of HFO, as shown in Table S1.

Table 1
Major technical specifications of the main and auxiliary diesel engines.

Specifications	Main engine	Auxiliary engine
Engine type	2-stroke diesel engine	4-stroke diesel engine
Model	MAN B&W 6S50ME-C8	MAN B&W 6L16/24
Power	7948 kW	660 kW
Rotation rate	127 r·min^{-1}	1200 r·min^{-1}

The ship traveled from Huanghua port in Bohai Bay, China through the Bohai Sea, Yellow Sea, and East China Sea to the Yangtze River, eventually arriving at Zhenjiang port (See Fig. S1). Measurements were taken during various operational modes throughout the voyage, including at-berth, departure, cruising, and arrival. At-berth and arrival tests were each performed one time, while departure tests were performed twice, once while departing from Huanghua port and once while departing from an anchorage near the Yangtze Estuary. The ship features five cruising speed gears, namely "Max," "Full," "Half," "Slow," and "Dead Slow." During ocean and inland sailing, the gear was usually set between "Full" and "Max" to enhance economy; thus, most of the samples collected in the ocean and inland seas feature these operational modes. The impact of cruise speed on emissions was investigated by intentionally setting the ship to specific modes, including "Max," "Full," and "Half," during measurement. The operational modes and their corresponding speeds, engine rotation rates, engine loads, and specific fuel oil consumption (SFOC) rates are presented in Table S2.

2.2. Sampling and analysis

A schematic of the sampling apparatus is shown in Fig. 1. The sampling instruments were placed on a deck below the chimneys. Exhaust gas was diverted to the deck through a stainless-steel air duct 108 mm in diameter; to avoid particle precipitation due to thermophoresis, the exterior of the air duct was wrapped in thermal insulation. Two sampling inlets were installed at the end of the air duct approximately 15 m downstream from the chimney. The

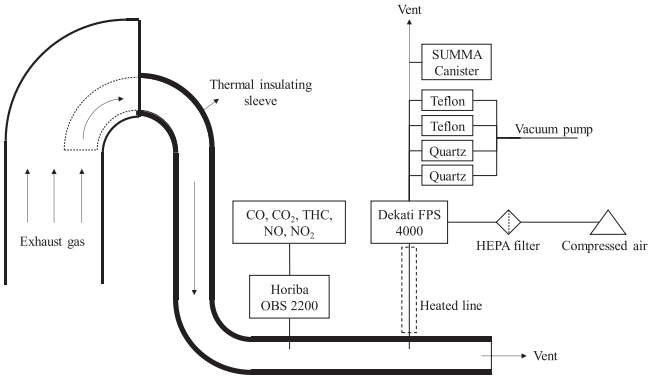

Fig. 1. Schematic diagrams of sampling setup.

first sampling inlet was connected to a Horiba OBS 2200 Portable Emission Measurement System (PEMS) for continuous gas monitoring. The PEMS system uses a non-dispersive infrared (NDIR) analyzer to measure CO and CO_2, a chemiluminescent detection (CLD) analyzer to measure NO and NO_2, and a flame ionization detector (FID) to measure total hydrocarbons (THC). The FID was calibrated using a propane gas standard with a concentration of 2035 ppm. The second sampling inlet was connected to a Dekati FPS 4000 dilution system for PM and VOC analysis. Samples were extracted from the raw exhaust gas using a perforated probe heated to 150 °C. Subsequently, the samples were diluted with HEPA-filtered compressed air in two stages. The primary dilution was performed using a perforated tube heated to 150 °C; within the tube, dilution air was introduced through small pores along a transport line in order to minimize losses inside the probe. The second dilution stage was performed with an ejector diluter, which pulled diluted sample flow from the primary dilution. The dilution ratio (DR) for each test is shown in Table S2.

After dilution, PM was sampled using four separate filter trains. Two Teflon filters (47 mm, TE38, Whatman, UK) and two quartz filters (47 mm, QM-A, Whatman, UK) were used during each measurement period; one filter was placed in each of the four channels. The flow rate through each channel was 5 L min^{-1}. To determine the emitted PM mass, the Teflon filters were analyzed gravimetrically after equilibration at 20 ± 1 °C and 50 ± 5% relative humidity for 24 h. After gravimetric analysis, one Teflon filter sample was extracted and analyzed for water soluble ions using an ion chromatograph (model 940, Metrohm, Switzerland); Fig. S2 shows balance between anions and cations in all samples. The other Teflon filter was analyzed for elemental content using an energy-dispersive X-ray fluorescence spectrometer (ED-XRF, Epsilon 5, PANalytical, Finland). One quartz filter sample was analyzed for OC and EC using a Desert Research Institute Thermal/Optical Carbon Analyzer Model 2001 and the IMPROVE-A protocol (Chow et al., 2007). The other quartz filter was analyzed for solvent-extractable organic compounds (SEOC), including *n*-alkanes, hopanes, PAHs, and *n*-fatty acids, using a gas chromatograph-mass spectrometer (GC-MS, Agilent, USA); the analytical procedure has been described previously (Feng et al., 2007). Briefly, one-fourth of the quartz filter was spiked with a surrogate mixture consisting of tetracosane-d50, anthracene-*d10*, chrysene-*d12*, perylene-*d12*, and heptadecanoic acid-*d33*, after which the sample was ultrasonically extracted in three 60 mL aliquots of dichloromethane/methanol (2:1, V/V) at room temperature. The combined extract was filtered and then reacted with freshly prepared diazomethane to esterify the free organic acids. The total extract was then subjected to GC-MS analysis (Agilent 5975 MSD interfaced with an Agilent 6890 gas chromatograph). Hexamethyl benzene was added prior to GC-MS analysis as an internal standard for *n*-alkanols and to verify the recovery of alkanes, PAHs, and fatty acids; alkanes, PAHs, and fatty acids were quantified using deuterated internal standards with chemical characteristics and retention times similar to the target analytes. The MS analysis covered a mass range of *m/z* 45–550 in electron impact mode at 70 eV. The GC, which features a HP-5MS capillary column (30 m × 0.25 mm × 0.25 μm), was operated with helium carrier gas at a flow rate of 1.0 mL min^{-1}. Analytes were quantified using linear regressions from five-point calibration curves established between authentic-standard-to-internal-standard concentrations ratios and the corresponding peak area ratios.

VOC species in the diluted exhaust were determined using SUMMA canister samples, which were analyzed offline for individual C2 to C12 hydrocarbons using a gas chromatograph with a mass spectrometer and flame ionization detector (GC-MS/FID). First, VOC samples were transferred into a cryogenic pre-concentrator (TH_PKU-300, Tianhong, China) and concentrated at −150 °C by two traps. The concentrated VOCs were desorbed at 100 °C and injected into the gas chromatograph (GC2010, Shimadzu, Japan), in which C2-C5 hydrocarbons were separated on a PLOT capillary column (0.32 mm × 15 m, Dikma, USA) and quantified by the FID. C5-C10 hydrocarbons and oxygenated VOCs (OVOCs) were separated on a DB-624 column (0.25 mm × 60 m, Agilent, USA) and quantified using a quadrupole mass spectrometer (GCMS-QP2010E, Shimadzu, Japan); the MS was operated with a source temperature of 200 °C over a mass range of *m/z* 30–300.

2.3. Calculation of emission factors

Emissions data are reported as power- or distance-based based EFs, which can be calculated from the measured pollutant concentrations using the following equations:

$$EF_{i,\ power-based} = \frac{EF_{i,fuel-based} \times Fuel\ Consumption}{Engine\ Power} = \frac{\Delta m_i \times x_c}{\Delta CO_2 + \Delta CO + \Delta PM_c + \Delta THC} \times \frac{Fuel\ Consumption}{Engine\ Power} \quad (1)$$

$$EF_{i,distance-based} = \frac{EF_{i,fuel-based} \times Fuel\ Consumption}{Distance} = \frac{\Delta m_i \times x_c}{\Delta CO_2 + \Delta CO + \Delta PM_c + \Delta THC} \times \frac{Fuel\ Consumption}{Speed \times \Delta t} \quad (2)$$

where $EF_{i,power\text{-}based}$, $EF_{i,fuel\text{-}based}$, and $EF_{i,distance\text{-}based}$ are the power- (g·kWh^{-1}), fuel- (g·kg^{-1}), and distance-based EFs (g·nautical mile^{-1}, or g·nmi^{-1}), respectively, of species *i*. Δm_i is the measured mass concentration of species *i* in the exhaust gas (mg·m^{-3}), x_c is the mass fraction of carbon (%) in the fuel as determined by fuel analysis (see Table S1), and ΔCO_2, ΔCO, ΔPM_c, and ΔTHC are the background-corrected carbon concentrations of CO_2, CO, carbonaceous PM, and THC (gC·m^{-3}). *Fuel Consumption* (kg·h^{-1}) and *Engine Power* (kW) data were obtained from the ship instrumentation. Distance was calculated based on the vessel speed (knots) and travel time (Δt). NO_x emissions, which consist of both NO and NO_2, were dominated by NO, so the molecular weight of NO was used in the NO_x EF calculations.

3. Results and discussion

3.1. Gaseous and particle emissions

The EFs found herein for NO_x, CO, THC, PM, and CO_2 are summarized in Table 2, together with data from the literature. The EFs measured in this study were generally similar to the literature values; the variations in the EFs can be attributed largely to differences in engine type, operating conditions, and fuel characteristics. Ship NO_x, CO, THC, and PM emissions were related primarily to engine power; NO_x and PM emissions increased linearly with increasing engine power, while CO and THC emissions decreased (Fig. S3). The auxiliary engine possessed the lowest NO_x EF. When the engine power was <10,000 kW at 50% load, the NO_x emission levels were 33% lower than estimates (18 g·kWh^{-1}) from the U.S. EPA (2009) and California Air Resources Board (CARB, 2008), which could lead to overestimation of NO_x emissions from ships in existing emission inventories.

Table 2
Gaseous and particulate emission factors from this and previous studies.

Studies	Engines	Engine power (kW)	HFO (% S)	Operation modes	Engine loads (%)	NO_x ($g \cdot kWh^{-1}$)	CO ($g \cdot kWh^{-1}$)	THC ($g \cdot kWh^{-1}$)	PM ($g \cdot kWh^{-1}$)	CO_2 ($g \cdot kWh^{-1}$)
This study	Auxiliary engine	660	0.38	At-berth	50	4.58	1.33	0.29	0.74	904.48
	Main engine	7948	0.38	Departure 1	0–50	8.74	2.89	0.51	1.08	746.23
			1.12	Departure 2	0–50	10.50	3.35	0.27	1.23	722.75
				Arrival	50–0	15.05	6.78	0.55	0.65	601.70
				Cruising	74	7.73	2.09	0.16	0.76	607.39
					51 ± 4	8.48 ± 0.44	2.77 ± 0.69	0.26 ± 0.04	0.68 ± 0.25	644.34 ± 30.05
					36	9.49	2.53	0.27	0.89	602.02
					15	14.69 ± 1.21	3.24 ± 1.44	0.30 ± 0.07	1.17 ± 0.10	696.96 ± 53.85
Agrawal et al. (2008a)	Main engine	50270	2.05	Cruising	8	20.96	1.78	–	1.70	660
					27	15.84	1.81	–	1.09	588
					52	16.40	0.87	–	1.39	613
					63	17.85	0.81	–	1.66	643
					70	18.89	0.77	–	1.76	658
Moldanová et al. (2009)	Main engine	20200	1.97	Cruising	84	14.22	0.42	0.07	1.03	667
Winnes and Fridell (2009)	Main engine	4500	1.60	Cruising	50	7.49	1.05	0	–	620
					70	8.49	0.74	0	0.53	603
					90	10.71	0.3	0	0.69	607
Agrawal et al. (2010)	Main engine	54840	3.01	Cruising	60	19.77 ± 0.28	0.29 ± 0.02	–	2.40 ± 0.05	617 ± 11
Moldanová et al. (2013)	Main engine	4440	1.00	Cruising	30	9.6	1.82	0.27	0.35	678
					80	9.6	1.17	0.30	0.41	617
	Main engine	6000	1.00	Cruising	57	12.5	0.96	0.10	0.27	610
			0.50	Cruising	57	10.1	0.92	0.07	0.19	592
Celo et al. (2015)	Main engine	N/A	2.23	Cruising	70	16.3 ± 0.2	0.83 ± 0.01	–	1.51 ± 0.07	614 ± 1
	Main engine	N/A	1.22	Cruising	77	8.4 ± 0.03	1.31 ± 0.02	–	0.37 ± 0.01	609 ± 1
	Main engine	N/A	1.48	Cruising	85	11.4 ± 0.1	0.26 ± 0.01	–	0.81 ± 0.02	626 ± 7
			2.21	Cruising	85	11.3 ± 0.1	0.30 ± 0.01	–	0.94 ± 0.02	628 ± 9
	Main engine	N/A	1.62	Cruising	75	12.2 ± 0.01	0.81 ± 0.03	–	0.83 ± 0.01	628 ± 1
			0.12	Cruising	75	10.7 ± 0.04	1.22 ± 0.02	–	0.30 ± 0.03	622 ± 1
	Main engine	N/A	2.70	Cruising	85	16.7 ± 0.1	0	–	2.2 ± 0.2	605 ± 1
Chu-Van et al. (2017)	Main engine	6880	3.13	Maneuvering	0–65	8.15 ± 1.71	1.76 ± 0.93	0.14 ± 0.07	1.87 ± 0.85	627 ± 2.10
				Cruising	81	10.2 ± 0.33	0.98 ± 0.06	0.06 ± 0.01	1.0 ± 0.08	626 ± 0.08
	Auxiliary engine	425	3.13	At-berth	55	6.5 ± 0.05	1.14 ± 0.04	–	–	850 ± 0.02

The operational mode also influenced gaseous and particulate emissions from ships. The NO_x, CO, THC, PM, and CO_2 EFs measured herein during maneuvering (including departure and arrival) were 13%, 63%, 79%, 13%, and 8% higher, respectively, than those measured during cruising. During cruising, all of the gaseous and particulate EFs increased with decreasing engine load. Switching from HSF (1.12% S) to LSF (0.38% S) resulted in 17% and 12% reductions in NO_x and PM emissions under departure conditions. However, the emissions reductions due to fuel switching noted in this study were generally lower than those reported in previous studies (Lack et al., 2011; Jayaram et al., 2011; Sippula et al., 2014; Celo et al., 2015; Zetterdahl et al., 2016; Ntziachristos et al., 2016), likely because the LSF used in this study was essentially HFO, which does not meet the marine distillate oil requirements in North American and European emission control areas.

3.2. Speciated PM emissions

The fractional mass contributions of various PM chemical components and the EFs of the major PM species are shown in Fig. 2(a) and (b), respectively; the speciated PM EFs are summarized in Table S4. The PM emitted from the test ship featured large amounts of OC, with OC/PM mass fractions between 45% and 65%. The OC content was dominated by the highly volatile OC1 and OC2 fractions, while the OC emission levels were influenced by the fuel type and engine mode. The OC EFs at-berth and during maneuvering were 31% higher than those measured during cruising. It should be noted that the dilution ratios at-berth and during departure (~64–1) were much higher than those under other operating conditions (~8–1), which may have shifted the OC gas-particle equilibrium toward the gas phase. Thus, the OC emissions at-berth and during departure should be higher than those during other operational modes if measured at the same dilution ratio. During cruising, the OC EF increased with decreasing engine load. During maneuvering, the OC EF for the main engine was 33% higher when fueled by HSF than when fueled by LSF.

EC emissions depended primarily on the engine type. The EC/PM mass fraction from the auxiliary engine was 20%, while that from the main engine ranged from only 1%–6%. The EC EF for the auxiliary engine was 6.7 times the average EF for the main engine. This variation in the main engine EC EF, which was caused by changes in the fuel and operational mode, differs from that observed for OC. The EC EF tended to decrease with decreasing engine load and then significantly increase at 15% engine load. As in previous studies, switching from HSF to LSF did not reduce EC emissions (Sippula et al., 2014; Celo et al., 2015).

Ionic components accounted for 8%–27% of the PM emissions, and sulfate was the most abundant component. The sulfate fraction increased from 2.7% to 12.2% when switching from LSF to HSF. As shown in Fig. 2(b), the sulfate EF of the ship during maneuvering was 3.4 times higher using HSF than using LSF. During cruising, the sulfate EF from the main engine first decreased, then increased with increasing engine load. Beyond sulfate, the ionic content consisted largely of Ca^{2+}, NH_4^+, NO_2^-, NO_3^-, and PO_4^{3-}, which accounted for 3.1%, 2.2%, 1.3%, 1.3%, and 0.9% of mass, respectively.

The elemental composition of the PM also depended strongly on fuel type. V and Ni dominated emissions from HSF but were found in much lower concentrations in LSF emissions, which consisted primarily of Si, Fe, Sn, Ba, Al, and Zn. During maneuvering, switching from HSF to LSF reduced the EFs of V and Ni by 85% and

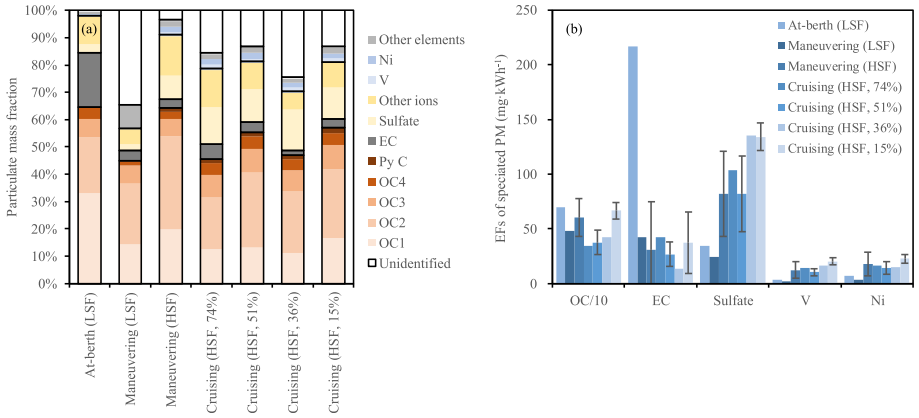

Fig. 2. (a) PM mass fractions contributed by various species and (b) EFs of speciated PM components under different operational modes. Maneuvering (LSF) indicates a departure operation using low-sulfur fuel. Maneuvering (HSF) includes departure and arrival operations using high-sulfur fuel. Cruising includes four different engine loads during sailing in the ocean and inland. OC1-OC4 denote organic carbon fractions, and Py C is the pyrolytic carbon fraction revealed by the IMPROVE-A protocol used in the thermal-optical carbon analysis. Other ions include speciated ionic components excluding sulfate, while Other elements include elements with the exception of V and Ni.

80%, respectively. The trends in V and Ni emissions with increasing engine load were similar to those noted for sulfate: first decreasing, then increasing. The use of HSF and LSF produced V:Ni ratios of 0.80 ± 0.16 and 0.49 ± 0.03, respectively, which are slightly lower than those measured by Celo et al. (2015). However, these V:Ni ratios are not consistent with the commercial shipping emission V:Ni tracer recommended by Viana et al. (2009). The HSF and LSF V:EC ratios were 0.53 ± 0.36 and 0.033 ± 0.020, respectively; the HSF ratio is consistent with the recommended tracer (Viana et al., 2009), while the LSF ratio is much lower. Generally, the ship emission tracers recommended by Viana et al. (2009) are inconsistent with those found herein, especially for ships fueled with LSF.

3.3. Particulate organic matter

The fractional contributions of various particulate organic matter (POM) species to total organics are shown in Fig. 3(a). Altogether, 21 *n*-alkanes, 10 hopanes, 21 particulate PAHs, and 27 *n*-fatty acids were quantified in the PM samples (see Table S5 for the EFs); these species contributed approximately 2–7% of the total organic mass on the filter. Fuel type heavily impacts the POM composition. When using LSF instead of HSF, the ship emitted much lower proportions of *n*-alkanes, hopanes, and PAHs, but higher amounts of *n*-fatty acids. The *n*-alkanes emitted from LSF consisted primarily of C18-C23 compounds, while HSF emitted a broader distribution of alkanes and more high-carbon components (such as C27-C36), as shown in Fig. S4(a). Hopanes can be used as organic tracers for oil combustion processes. The hopane fractions were consistent between the two fuels; the most abundant hopanes were 17a(H)21β(H)-hopane (C30H) and 17a(H)21β(H)-30-Norhopane (C29H) (see Fig. S4(b)).

The particulate PAH EFs were classified by the number of benzene rings in the given PAH, as shown in Fig. 3(b). Fueling the main engine with LSF (as opposed to HSF) during maneuvering decreased particulate PAH emissions by 94%; these decreases were most evident in PAHs with 3 and 4 rings, including fluoranthene, acephenanthrene, pyrene, benzo[ghi]fluoranthene, cyclopenta[cd]pyrene, chrysene, and benzo[b+k]fluoranthene. The operational mode of the ship also influenced particulate PAH emissions. The average EF measured during maneuvering was 3.6 times the average EF measured during cruising, and the cruising EFs generally increased with decreasing engine loads. Compounds with 3 and 4 aromatic rings accounted for 33–58% and 29–54%, respectively, of the particulate PAHs emitted by the various fuels and operational

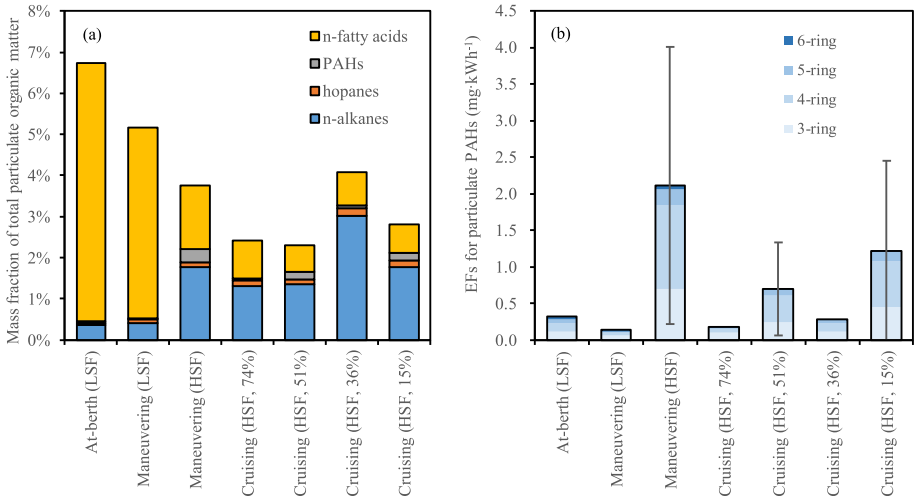

Fig. 3. (a) Fractional contributions of particulate organic matter species to total organic mass and (b) EFs of particulate PAHs from various operational modes. The PAHs are classified according to the number of benzene rings.

modes and included phenanthrene, fluoranthene, pyrene, and benzo[b+k]fluoranthene. The mass fractions of 5- and 6-ringed compounds, such as benzo[ghi]perylene, dibenz[ah]anthracene, and coronene, were higher in the LSF samples than in the HSF samples, as shown in Fig. S4(c).

The average *n*-fatty acid EF from LSF was 6.7 times that from HSF. However, the fractional contributions of various compounds to total *n*-fatty acid mass were quite similar between the two fuels (see Fig. S4(d)). Palmitic acid (C16:0) and octadecanoic acid (C18) were the most abundant compounds, contributing 57% and 22% of the total *n*-fatty acid mass, respectively.

3.4. VOC species emissions

Twenty-eight alkanes, 19 alkenes, acetylene, 16 single-ring aromatics, and 23 oxygenated VOCs (OVOCs) were quantified in the VOC samples (see Table S6 for the EFs). The VOC species mass fractions are shown in Fig. 4(a). The VOCs emitted from the different engines, fuel types, and operational modes were relatively similar. Single-ring aromatics dominated the VOCs in the ship exhaust tested herein, accounting for 50–74% in various samples. Alkanes, alkenes, and OVOCs contributed 7–22%, 4–7%, and 10–24%, respectively, of the VOC mass. The EFs of speciated single-ring aromatics are shown for various operational modes in Fig. 4(b). Fuel type had the most prominent influence on emissions of single-ring aromatics. The average EF for the main engine during maneuvering was 4.8 times higher with LSF than with HSF; this difference is consistent with the THC emissions (see Table 1) and likely arose from the fact that the engine is optimized for HFO operation, which may cause lower LSF combustion efficiency. Furthermore, sulfur in the fuel may have acted as a radical scavenger during combustion, reducing the formation of volatile aromatics via hydrogen-abstraction-carbon-addition (HACA) (Streibel et al., 2015).

Toluene was the most abundant of the single-ring aromatics. The LSF and HSF toluene EFs were 42.7 ± 21.2 mg·kWh^{-1} and 4.5 ± 7.2 mg·kWh^{-1} on average, accounting for 10.5 ± 1.3% and 1.6 ± 2.6% of the THC emissions. These values are similar to the toluene EFs (13.3 ± 2.2 mg·kWh^{-1}) measured by Radischat et al. (2015), whose study also indicated that switching from HFO to DF at low engine load increased toluene emissions. The results herein indicate considerable amounts of single-ring aromatics in the ship exhaust, which may contribute to the formation of ground-level ozone, especially in coastal areas.

3.5. EFs under different operating conditions

During cruising at sea, air pollutant emissions from ships are controlled primarily by the vessel speed and corresponding engine load. Fig. 5 presents relationships between the power-based and distance-based EFs of gaseous and particulate species measured herein under various engine loads and vessel speeds. With the exception of PM, EC, and sulfate, the power-based EFs of the gaseous and particulate species tended to decrease with increasing engine loads. PM, EC, and sulfate emissions were minimized at 30–40% engine loads and increased under low- and high-load conditions. Vessel speed increased with increasing engine load, as one might imagine. The vessel traveled at speeds of 5.4, 8.6, 9.2, and 11.3 knots under engine loads of 15%, 36%, 51%, and 74%, respectively. The distance-based EFs of the gaseous and particulate components decreased with decreasing vessel speed. A Vessel Speed Reduction (VSR) from 11 to 8–9 knots reduced NO_x and PM emissions by approximately 33% and 36%, respectively, while OC, EC, sulfate, and particulate PAH emissions in PM decreased by 34%, 83%, 29%, and 11%. Benzene, toluene, ethylbenzene, and xylene (BTEX) emissions did not change significantly with vessel speed. These results indicate that VSR can effectively decrease emissions of major particulate and gaseous pollutants from ships, which is consistent with previous studies (Lack et al., 2011; Khan et al., 2012).

4. Conclusions

This study presents detailed measurements of particulate and gaseous chemical emissions from the main and auxiliary engines of a Handysize-class bulk carrier operating under real-world conditions, including at-berth, maneuvering, and cruising. The EFs of PM components, VOC species, and criteria pollutants (including NO_x, CO, THC, and PM) were determined while the ship was burning LSF and HSF under different operating conditions. OC was the most abundant particle component, contributing 45–65% of the total PM mass, followed by sulfate and EC, which accounted for 2–15% and 1–20%, respectively. POM species, including *n*-alkanes, hopanes, particulate PAHs, and *n*-fatty acids, contributed approximately 2–7% of the total organic mass on the filter. Compounds with 3 or 4 aromatic rings, including phenanthrene, fluoranthene, pyrene, and benzo[b+k]fluoranthene, dominated the emitted particulate PAH species, accounting for 69%–89% of the total particulate PAHs. Single-ring aromatics were the most abundant VOC components,

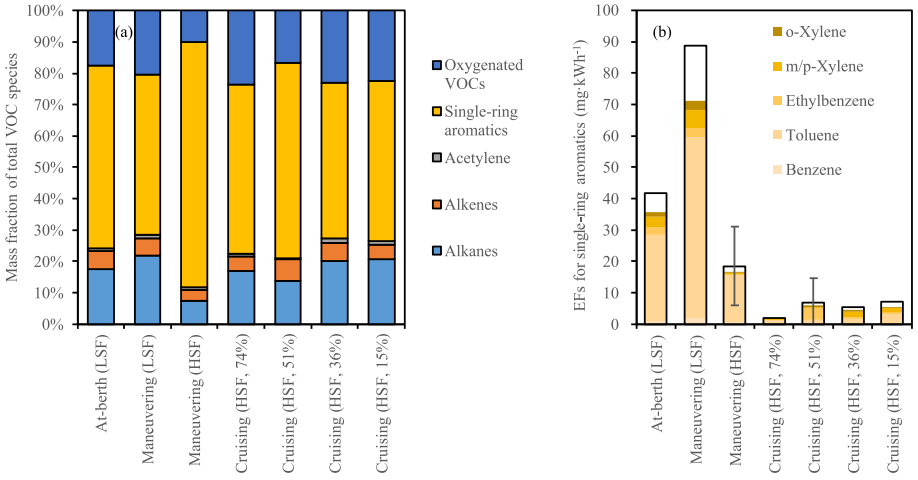

Fig. 4. (a) Fractional contributions of speciated VOCs to total VOC mass and (b) EFs of speciated aromatics from various operational modes.

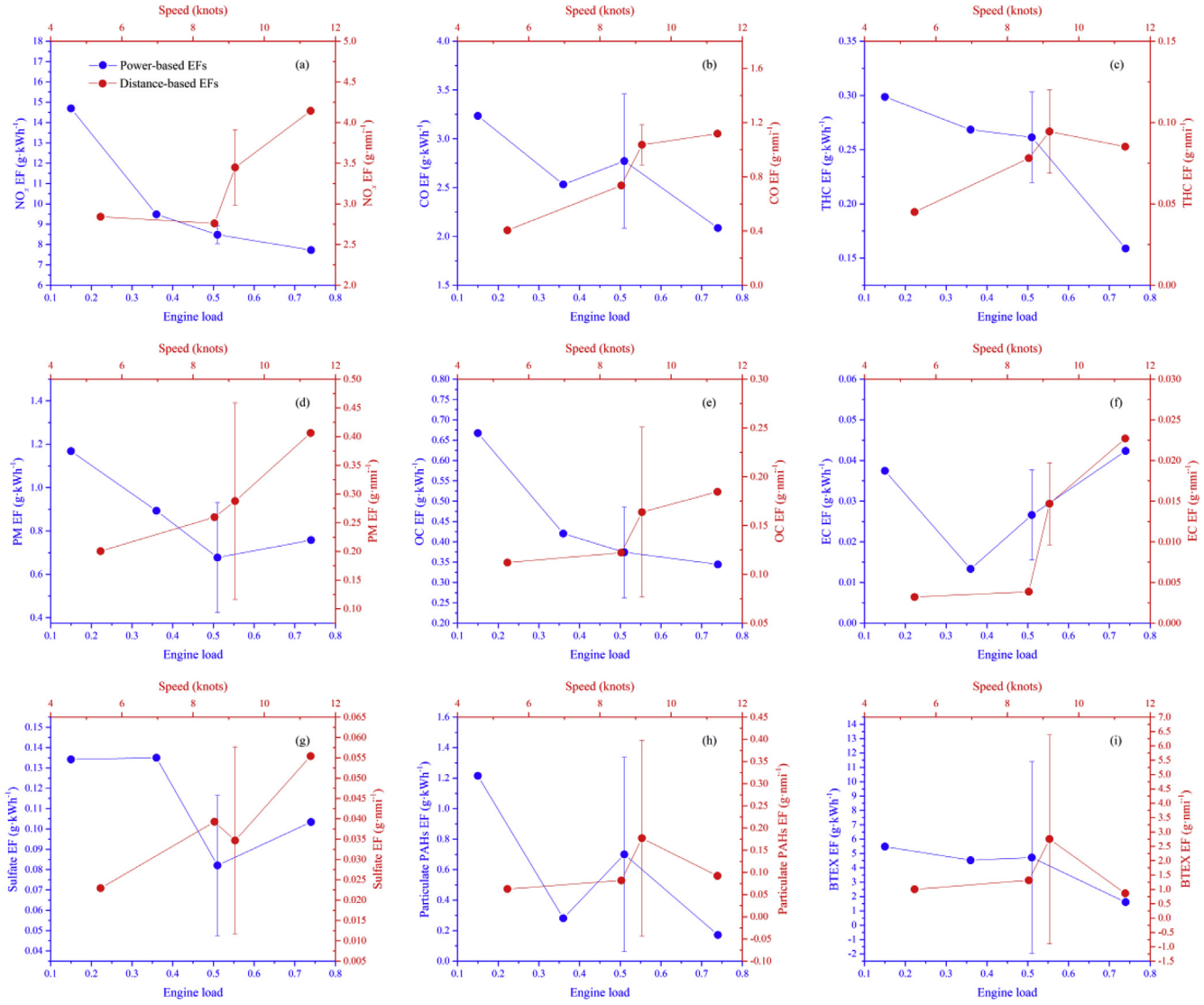

Fig. 5. EFs of gaseous and particulate pollutants from the main engine during cruising under different engine loads (blue) and vessel speeds (red). EFs are shown for (a) NO_x, (b) CO, (c) THC, (d) PM, (e) OC, (f) EC, (g) sulfate, (h) particle-bound PAHs, and (i) BTEX. BTEX encompasses the major single-ring aromatics, including benzene, toluene, ethylbenzene, m/p-xylene, and o-xylene. (For interpretation of the references to colour in this figure legend, the reader is referred to the Web version of this article.)

accounting for 50–74% of mass in various samples, and toluene was the dominant VOC species.

Fuel quality greatly affected PM emissions and composition. Switching from HSF (1.12% S) to LSF (0.38% S) reduced the emitted PM by ~12%, OC by 20%, sulfate by 71%, and particulate PAHs by 94%; however, VOC emissions were higher when the ship was fueled with LSF than when the ship was fueled with HSF. Moreover, fuel switching had no effect on EC emissions. The operational mode also influenced ship emissions. EFs for both particulate and gaseous compounds were higher during maneuvering than during cruising. During cruising, the majority of the power-based EFs decreased with increasing engine loads. The EFs of select pollutants, such as PM, EC, and sulfate, were minimized at engine loads of 30–40%. The results also indicate that VSR can decrease particulate and gaseous emissions. A VSR from the regular cruise speed of the ship (11 knots at 50% engine load) to 8–9 knots reduced NO_x and PM emissions by approximately 33% and 36%, respectively, and OC, EC, sulfate, and particulate PAHs emissions in PM by 34%, 83%, 29%, and 11%. This study aimed to quantify and chemically characterize emissions from ocean-going ships under real-world operating conditions in order to enhance the relevant databases and improve the accuracy of ship emission inventories. However, additional measurements are needed to minimize the uncertainties remaining in ship emissions estimations due to a lack of emission data.

Acknowledgments

The authors gratefully acknowledge Shanghai Maritime University for their support of the measurement. The authors would like to acknowledge the outstanding support received from all employees and crew of Yuming ship. This work was supported by the National Natural Science Foundation of China (Grant No. 21777101), the National Non-profit Scientific Research Program for Environmental Protection (Grant No. 201509005), the Shanghai Natural Science Fund (Grant No. 18ZR1432100), and the Shanghai Pujing Talent Plan (Grant No. 18PJ1431400).

Appendix A. Supplementary data

Supplementary data related to this article can be found at

https://doi.org/10.1016/j.envpol.2018.07.036.

References

Agrawal, H., Malloy, Q.G.J., Welch, W.A., Miller, J.W., Cocker III, D.R., 2008a. In-use gaseous and particulate matter emissions from a modern ocean going container vessel. Atmos. Environ. 42, 5504–5510.

Agrawal, H., Welch, W.A., Miller, J.W., Cocker, D.R., 2008b. Emission measurements from a crude oil tanker at sea. Environ. Sci. Technol. 42 (19), 7098–7103.

Agrawal, H., Welch, W.A., Henningsen, S., Miller, J.W., Cocker III, D.R., 2010. Emissions from main propulsion engine on container ship at sea. J. Geophys. Res. Atmos. 115. D23205.

Aksoyoglu, S., Baltensperger, U., Prévôt, A.S.H., 2016. Contribution of ship emissions to the concentration and deposition of air pollutants in Europe. Atmos. Chem. Phys. 16 (4), 1895–1906.

Becagli, S., Anello, F., Bommarito, C., Cassola, F., Calzolai, G., di Iorio, T., di Sarra, A., Gómez-Amo, J., Lucarelli, F., Marconi, M., Meloni, D., Monteleone, F., Nava, S., Pace, G., Severi, M., Sferlazzo, D.M., Traversi, R., Udisti, R., 2017. Constraining the ship contribution to the aerosol of the central Mediterranean. Atmos. Chem. Phys. 17 (3), 2067–2084.

Brandt, J., Silver, J.D., Christensen, J.H., Andersen, M.S., Bønløkke, J.H., Sigsgaard, T., Geels, C., Gross, A., Hansen, A.B., Hansen, K.M., Hedegaard, G.B., Kaas, E., Frohn, L.M., 2013. Assessment of past, present and future health-cost externalities of air pollution in Europe and the contribution from international ship traffic using the EVA model system. Atmos. Chem. Phys. 13 (15), 7747–7764.

Broome, R.A., Cope, M.E., Goldsworthy, B., Goldsworthy, L., Emmerson, K., Jegasothy, E., Morgan, G.G., 2016. The mortality effect of ship-related fine particulate matter in the Sydney greater metropolitan region of NSW, Australia. Environ. Int. 87, 85–93.

CARB, 2008. Emissions Estimation Methodology for Ocean-going Vessels (Available at http://www.arb.ca.gov/regact/2008/fuelogv08/appdfuel.pdf.

Celo, V., Dabek-Zlotorzynska, E., McCurdy, M., 2015. Chemical characterization of exhaust emissions from selected Canadian marine vessels: the case of trace metals and lanthanoids. Environ. Sci. Technol. 49 (8), 5220–5226.

Chow, J.C., Watson, J.G., Chen, L.W.A., Chang, M.C.O., Robinson, N.F., Trimble, D., Kohl, S., 2007. The IMPROVE_A temperature protocol for thermal/optical carbon analysis: maintaining consistency with a long-term database. J. Air Waste Manag. Assoc. 57, 1014–1023.

Chu-Van, T., Ristovski, Z., Pourkhesalian, A.M., Rainey, T., Garaniya, V., Abbassi, R., Jahangiri, S., Enshaei, H., Kam, U., Kimball, R., Yang, L.P., Zare, A., Bartlett, H., Brown, R.J., 2017. On-board measurements of particle and gaseous emissions from alarge cargo vessel at different operating conditions. Environ. Pollut. 237, 832–841.

Czech, H., Stengel, B., Adam, T., Sklorz, M., Streibel, T., Zimmermann, R., 2017. A chemometric investigation of aromatic emission profiles from a marine engine in comparison with residential wood combustion and road traffic: implications for source apportionment inside and outside sulphur emission control areas. Atmos. Environ. 167, 212–222.

Diesch, J.M., Drewnick, F., Klimach, T., Borrmann, S., 2013. Investigation of gaseous and particulate emissions from various marine vessel types measured on the banks of the Elbe in Northern Germany. Atmos. Chem. Phys. 13 (7), 3603–3618.

ENTEC UK Limited, 2002. Quantification of Emissions from Ships Associated with Ship Movements between Ports in the European Community, FS 13881. Eur. Comm (Brussels, Belgium).

Eyring, V., Isaksen, I.S.A., Berntsen, T., Collins, W.J., Corbett, J.J., Endresen, O., Grainger, R.G., Moldanova, J., Schlager, H., Stevenson, D.S., 2010. Transport impacts on atmosphere and climate: Shipping. Atmos. Environ. 44, 4735–4771.

Feng, J.L., Guo, Z.G., Chan, C.K., Fang, M., 2007. Properties of organic matter in $PM_{2.5}$ at Changdao Island, China-a rural site in the transport path of the Asian continental outflow. Atmos. Environ. 41, 1924–1935.

Gaston, C.J., Quinn, P.K., Bates, T.S., Gilman, J.B., Bon, D.M., Kuster, W.C., Prather, K.A., 2013. The impact of shipping, agricultural, and urban emissions on single particle chemistry observed aboard the R/V Atlantis during CalNex. J. Geophys. Res. Atmos. 118 (10), 5003–5017.

Jayaram, V., Agrawal, H., Welch, W.A., Miller, J.W., Cocker III, D.R., 2011. Real-time gaseous, PM and ultrafine particle emissions from a modern marine engine operating on biodiesel. Environ. Sci. Technol. 45 (6), 2286–2292.

Johansson, L., Jalkanen, J., Kukkonen, J., 2017. Global assessment of shipping emissions in 2015 on a high spatial and temporal resolution. Atmos. Environ. 167, 403–415.

Khan, M.Y., Agrawal, H., Ranganathan, S., Welch, W.A., Miller, J.W., Cocker III, D.R., 2012. Greenhouse gas and criteria emission benefits through reduction of vessel speed at sea. Environ. Sci. Technol. 46 (22), 12600–12607.

Khan, M.Y., Ranganathan, S., Agrawal, H., Welch, W.A., Laroo, C., Miller, J.W., Cocker III, D.R., 2013. Measuring in-use ship emissions with international and U.S. federal methods. J. Air Waste Manag. Assoc. 63 (3), 284–291.

Lack, D.A., Cappa, C.D., Langridge, J., Bahreini, R., Buffaloe, G., Brock, C., Cerully, K., Coffman, D., Hayden, K., Holloway, J., Lerner, B., Massoli, P., Li, S.M., McLaren, R., Middlebrook, A.M., Moore, R., Nenes, A., Nuaaman, I., Onasch, T.B., Peischl, J., Perring, A., Quinn, P.K., Ryerson, T., Schwartz, J.P., Spackman, R., Wofsy, S.C., Worsnop, D., Xiang, B., Williams, E., 2011. Impact of fuel quality regulation and speed reductions on shipping emissions: implications for climate and air quality. Environ. Sci. Technol. 45 (20), 9052–9060.

Lack, D.A., Corbett, J.J., 2012. Black carbon from ships: a review of the effects of ship speed, fuel quality and exhaust gas scrubbing. Atmos. Chem. Phys. 12 (9), 3985–4000.

Lehtoranta, K., Vesala, H., Koponen, P., Korhonen, S., 2015. Selective catalytic reduction operation with heavy fuel oil: NO_x, NH_3, and particle emissions. Environ. Sci. Technol. 49 (7), 4735–4741.

Liu, H., Fu, M.L., Jin, X.X., Shang, Y., Shindell, D., Faluvegi, G., Shindell, C., He, K.B., 2016. Health and climate impacts of ocean-going vessels in East Asia. Nat. Clim. Change 6 (11), 1037–1041.

Liu, Z.M., Lu, X.H., Feng, J.L., Fan, Q.Z., Zhang, Y., Yang, X., 2017. Influence of ship emissions on urban air quality: a comprehensive study using highly time-resolved online measurements and numerical simulation in Shanghai. Environ. Sci. Technol. 51 (1), 202–211.

Manoli, E., Chelioti-Chatzidimitriou, A., Karageorgou, K., Kouras, A., Voutsa, D., Samara, C., Kampanos, I., 2017. Polycyclic aromatic hydrocarbons and trace elements bounded to airborne PM_{10} in the harbor of Volos, Greece: implications for the impact of harbor activities. Atmos. Environ. 167, 61–72.

Marelle, L., Thomas, J.L., Raut, J., Law, K.S., Jalkanen, J., Johansson, L., Roiger, A., Schlager, H., Kim, J., Reiter, A., Weinzier, B., 2016. Air quality and radiative impacts of Arctic shipping emissions in the summertime in northern Norway: from the local to the regional scale. Atmos. Chem. Phys. 16 (4), 2359–2379.

Moldanová, J., Fridell, E., Popovicheva, O., Demirdjian, B., Tishkova, V., Faccinetto, A., Focsa, C., 2009. Characterisation of particulate matter and gaseous emissions from a large ship diesel engine. Atmos. Environ. 43, 2632–2641.

Moldanová, J., Fridell, E., Winnes, H., Holmin-Fridell, S., Boman, J., Jedynska, A., Tishkova, V., Demirdjian, B., Joulie, S., Bladt, H., Ivleva, N.P., Niessner, R., 2013. Physical and chemical characterisation of PM emissions from two ships operating in European emission control areas. Atmos. Meas. Tech. 6, 3577–3596.

Ntziachristos, L., Saukko, E., Lehtoranta, K., Rönkkö, T., Timonen, H., Simonen, P., Karjalainen, P., Keskinen, J., 2016. Particle emissions characterization from a medium-speed marine diesel engine with two fuels at different sampling conditions. Fuel 186, 456–465.

Olivié, D.J.L., Cariolle, D., Teyssèdre, H., Salas, D., Voldoire, A., Clark, H., Saint-Martin, D., Michou, M., Karcher, F., Balkanski, Y., Gauss, M., Dessens, O., Koffi, B., Sausen, R., 2012. Modeling the climate impact of road transport, maritime shipping and aviation over the period 1860–2100 with an AOGCM. Atmos. Chem. Phys. 12 (3), 1449–1480.

Pitchford, M., Malm, W., Schichtel, B., Kumar, N., Lowenthal, D., Hand, J., 2007. Revised algorithm for estimating light extinction from IMPROVE particle speciation data. J. Air Waste Manag. Assoc. 57 (11), 1326–1336.

Radischat, C., Sippula, O., Stengel, B., Klingbeil, S., Sklorz, M., Rabe, R., Streibel, T., Harndorf, H., Zimmermann, R., 2015. Real-time analysis of organic compounds in ship engine aerosol emissions using resonance-enhanced multiphoton ionization and proton transfer mass spectrometry. Anal. Bioanal. Chem. 407, 5939–5951.

Seinfeld, J.H., Pandis, S.N., 2006. Atmospheric Chemistry and Physics: from Air Pollution to Climate Change, second ed. Wiley, New York, pp. 265–266.

Sippula, O., Stengel, B., Sklorz, M., Streibel, T., Rabe, R., Orasche, J., Lintelmann, J., Michalke, B., Abbaszade, G., Radischat, C., Gröger, T., Schnelle-Kreis, J., Harndorf, H., Zimmermann, R., 2014. Particle emissions from a marine engine: chemical composition and aromatic emission profiles under various operating conditions. Environ. Sci. Technol. 48 (19), 11721–11729.

Streibel, T., Mühlberger, F., Geißler, R., Saraji-Bozorgzad, M., Adam, T., Zimmermann, R., 2015. Influence of sulphur addition on emissions of polycyclic aromatic hydrocarbons during biomass combustion. Environ. Sci. Technol. 49 (8), 5220–5226.

Tagaris, E., Stergiou, I., Sotiropoulou, R.P., 2017. Impact of shipping emissions on ozone levels over Europe: assessing the relative importance of the Standard Nomenclature for Air Pollution (SNAP) categories. Environ. Sci. Pollut. Res. 24 (17), 14903–14909.

Thomson, E.S., Weber, D., Bingemer, H.G., Tuomi, J., Ebert, M., Pettersson, J.B.C., 2018. Intensification of ice nucleation observed in ocean ship emissions. Sci. Rep. 8, 1111,. https://doi.org/10.1038/s41598-018-19297-y.

U.S.EPA, 2009. Current Methodologies in Preparing Mobile Source Port-related Emission Inventories. Final Report. Available at. http://www.epa.gov/cleandiesel/documents/ports-emission-inv-april09.pdf.

Velchev, K., Cavalli, F., Hjorth, J., Marmer, E., Vignati, E., Dentener, F., Raes, F., 2011. Ozone over the Western Mediterranean Sea – results from two years of shipborne measurements. Atmos. Chem. Phys. 11 (2), 675–688.

Viana, M., Amato, F., Alastuey, A., Querol, X., Moreno, T., García Dos Santos, S., Herce, A.D., Fernández-Patier, R., 2009. Chemical tracers of particulate emissions from commercial shipping. Environ. Sci. Technol. 43 (19), 7472–7477.

Winnes, H., Fridell, E., 2009. Particle emissions from ships: dependence on fuel type. J. Air Waste Manag. Assoc. 59 (12), 1391–1398.

Zetterdahl, M., Moldanová, J., Pei, X.Y., Pathak, R.K., Demirdjian, B., 2016. Impact of the 0.1% fuel sulfur content limit in SECA on particle and gaseous emissions from marine vessels. Atmos. Environ. 145, 338–345.